36th AIAA Fluid Dynamics Conference and Exhibit
5 - 8 June 2006, San Francisco, California

AIAA 2006-3904

Direct and Large-Eddy Simulation of Decaying and Forced Isotropic Turbulence Using Lattice Boltzmann Method

Juan Orphee [*], Ayse G. Gungor [†], Martin Sanchez_Rocha [‡], and Suresh Menon[§]

Georgia Institute of Technology,

Atlanta, GA, 30332-0150,

USA

The capability of the lattice Boltzmann method to simulate turbulent flows using direct and large eddy simulations is explored by performing decaying and forced isotropic turbulence. The decay exponents and the spectral scaling properties of energy and dissipation are compared with classical results. The lattice Boltzmann method, with single and multiple relaxation time, captures important features of turbulence, and the results are in agreement with the classical ones. The ability of the lattice Boltzmann method to perform large eddy simulation using dynamic Smagorinsky model and the local dynamic subgrid kinetic energy method is explored.

I. Introduction

The lattice Boltzmann equation (LBE) has become an alternative method for solving various fluid dynamic problems. By considering the LBE as a numerical approach to solve the Boltzmann equation, X. He and L. S. Luo,[1],[2] and A. Takashi,[3] set forth the theoritical foundation of the LBE method. The LBE has been successfully tested for different kind of problems, laminar to turbulent flows in two and three dimensions.[4,5,6] Commonly used, the lattice Boltzmann equation is the lattice Bhatnagar-Gross-Krook (LBGK) equation based on a single relaxation time (SRT). Although it has deficiencies, it has been the most popular model due to its simplicity. The multiple relaxation time (MRT)-LBE method, introduced by d'Humieres et.al[7] overcomes some of these deficiencies, such as fixed Prandtl number and fixed ratio between kinematic and bulk viscosities. The stability of the LBGK model has been improved by the MRT-LBE model by using different relaxation times of the moments. The linearized analysis of the MRT-LBE model (by Lallemand and Luo[8]) shows that the MRT-LBE gives the same results with second order accuracy when compared with the SRT-LBE models.

The MRT-LBE has shown to be an efficient model to simulate complex flows.[9] However, the simulation of high Reynolds number turbulent flows with LBE still remains to be fully explored. Direct numerical simulation (DNS) is computationally very expensive with LBE as well as with other conventional methods. Large eddy simulations (LES) is explored here using dynamic subgrid scale methods for the Reynolds stress closure. Two dynamic eddy viscosity models are used: a model based on Smagorinsky[10] eddy viscosity, and a model based on the subgrid-scale (SGS) kinetic energy (k^{sgs}).

The objective of this work is to conduct a DNS of decaying and forced homogeneous isotropic turbulence to validate the MRT-LBE method, and to study the K-eqn. SGS model to simulate high Reynolds number flows using LES.

[*]Undergraduate Research Assistant, AIAA Student Member.
[†]Graduate Research Assistant, AIAA Student Member.
[‡]Graduate Research Assistant, AIAA Student Member
[§]Professor, AIAA Associate Fellow.

II. Governing Equations and Numerical Methods

A. Governing Equations

The governing equation of the lattice Boltzmann is obtained by normalizing the Boltzmann equation with reference scales, achieving a non-dimensional form of the Boltzmann equation. These reference scales, denoted with a subscript "r," are as follows: l_r = reference length scale, c_r = reference velocity, ρ_r = reference density. Using reference scales, the non-dimensional variables are defined as $\hat{f} = f/\rho_r$, $\hat{c}_i = c_i/c_r$, $\hat{x}_j = x_j/l_r$, $\hat{\tau} = \tau/(\lambda/c_r)$ and $\hat{t} = t/(l_r/c_r)$. The lattice Boltzmann equation states that the number of particles with a velocity class $\hat{c}_i$ changes according to three processes: collision, convection, and acceleration. Therefore, the normalized Boltzmann equation according to these processes is

$$\frac{\partial \hat{f}}{\partial t} + \hat{c_j}\frac{\partial \hat{f}}{\partial \hat{x_j}} = -\frac{\hat{f} - \hat{f}_o}{\epsilon\hat{\tau}}. \tag{1}$$

where τ is the collision time, $\hat{f}_o$ is the equilibrium distribution function, λ is the mean free path of particles, $\hat{f} = \rho g$, ρ is the local density, ϵ is the Knudsen number (λ/l_r), and g is the particle distribution function, which represents the fraction of particles with a velocity class $\hat{c}_i$.

The first term of Eqn. 1, represents the rate of increase of particles with a $\hat{c}_i$ velocity class, the second term corresponds to the convection of particles across the control volume, and the third term represents the collision process among particles.

B. Numerical Methods

1. Single Relaxation Time Model

One of the main difficulties in the Boltzmann equation lies in identifying the appropriate collision time τ. This parameter was assumed constant under the assumption of small departures from equilibrium, known as the "$Bhatnagar - Gross - Krook$" collisional operator. Therefore, the evolution of the non-dimensional distribution function f (for the following the $\hat{f}$ is replaced by f) becomes

$$f_\alpha(x + e_\alpha\delta, t + \delta) - f_\alpha(x, t) = \frac{1}{\tau}[f_\alpha^{eq}(x, t) - f_\alpha(x, t)], \qquad \alpha = 0, 1, ..., 18, \tag{2}$$

where τ is the collision time, also referred to as the relaxation time, f_α^{eq} is the equilibrium distribution function, and e_α is the particle speed in the α direction. The characteristic speed is $c = e_\alpha\delta/\delta = |e_\alpha|$. Also, particles with zero velocity, rest particles with $e_0 = 0$, are allowed. Note that the time step and the lattice spacing each have equal spacing of unity. Thus, $\delta = 1$.

The three-dimensional 19-bit velocity field in the D3Q19 models, as shown in Figure 1, are

$$e_\alpha = \begin{cases} (0,0,0), & \alpha = \quad 0 \\ ((\pm1,0,0),(0,\pm1,0),(0,0,\pm1))c, & \alpha = \quad 1,2,..6 \\ ((\pm1,\pm1,0),(0,\pm1,\pm1),(\pm1,0,\pm1))\sqrt{2}c, & \alpha = \quad 7,8,...18 \end{cases} \tag{3}$$

Here, f_α^{eq} is given by the following form:

$$f_\alpha^{eq} = w_\alpha\rho\left[1 + \frac{3(e_\alpha.u)}{c^2} + \frac{9}{2}\frac{(e_\alpha.u)^2}{c^4} - \frac{3}{2}\frac{u^2}{c^2}\right], \tag{4}$$

where

$$w_\alpha = \begin{cases} \frac{1}{3}, & \alpha = \quad 0 \\ \frac{1}{18}, & \alpha = \quad 1,2,..6 \\ \frac{1}{36}, & \alpha = \quad 7,8,...18 \end{cases} \tag{5}$$

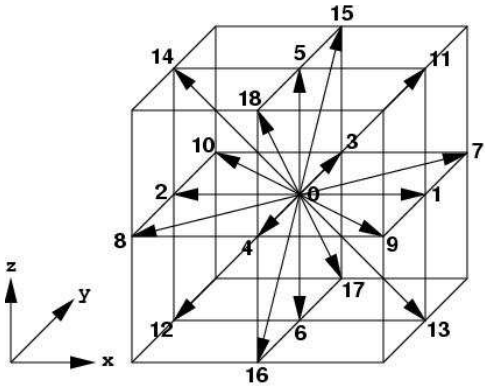

Figure 1. Link vectors of f_α.

2. Multiple Relaxation Time Model

In the SRT model, all moments relax to their equilibrium values with the same parameter. In contrast to the SRT approximation, the MRT model is based on different relaxation parameters for the moments. The evaluation of the equation for the distribution function with multiple relaxation times is written as

$$|f(x_i + e_\alpha \delta t, t + \delta t)\rangle - |f(x_i, t)\rangle = \quad - M^{-1}\hat{S}[|m(x_i, t)\rangle - |m^{eq}(x_i, t)\rangle]. \tag{6}$$

where M is the 19x19 transformation matrix (in all the studies here, a 19-velocity model is employed) mapping the distribution velocity vector $|f\rangle$ in discrete velocity space to a vector $|m\rangle$ in the moment space. The transformation matrix for D3Q19 model is given by d'Humieres et al.,[11] where the M matrix is modified appropriately for the velocity directions shown in Figure 1. In the MRT model, a set of new variables, or moments, which are related to the velocity vector in terms of the transformation matrix M is introduced as

$$|m\rangle = M|f\rangle \tag{7}$$

The corresponding 19 moments for D3Q19 model is given by

$$|m\rangle = (\rho, e, \varepsilon, j_x, q_x, j_y, q_y, j_z, q_z, 3P_{xx}, 3\pi_{xx}, P_{ww}, \pi_{ww}, P_{xy}, P_{yz}, P_{xz}, m_x, m_y, m_z)^T, \tag{8}$$

where ρ is the fluid density, e is the energy, ε is the square of the energy, j_x, j_y and j_z are the momentum densities, q_x, q_y and q_z are the energy fluxes, $p_{xx}, p_{ww}, p_{xy}, p_{yz}$ and p_{xz} are the symmetric traceless viscous stress tensors.

In the SRT model all the parameters are relaxed in the same manner, however, the relaxation procedure of the MRT for D3Q19 model is given by d'Humieres et al.[11] as

$$e^{eq} = -11\rho + \frac{19}{\rho_0} j.j \quad , \qquad \varepsilon^{eq} = \omega_\varepsilon \rho + \frac{\omega_{\varepsilon j}}{\rho_0} j.j \tag{9}$$

$$\mathrm{q}_x^{eq} = -\frac{2}{3} j_x, \qquad \mathrm{q}_y^{eq} = -\frac{2}{3} j_y, \qquad \mathrm{q}_z^{eq} = -\frac{2}{3} j_z \tag{10}$$

$$\mathrm{P}_{xx}^{eq} = \frac{1}{3\rho_0}\left[2\mathrm{j}_x^2 - \left(\mathrm{j}_y^2 + \mathrm{j}_z^2\right)\right] \quad , \quad \mathrm{P}_{ww}^{eq} = \frac{1}{\rho_0}\left[\mathrm{j}_y^2 - \mathrm{j}_z^2\right] \tag{11}$$

$$\mathrm{P}_{xy}^{eq} = \frac{1}{\rho_0} j_x j_y, \quad \mathrm{P}_{yz}^{eq} = \frac{1}{\rho_0} j_y j_z, \quad \mathrm{P}_{xz}^{eq} = \frac{1}{\rho_0} j_x j_z \tag{12}$$

$$\pi_{xx}^{eq} = \omega_{xx} \mathrm{P}_{xx}^{eq} \quad , \qquad \pi_{ww}^{eq} = \omega_{xx} \mathrm{P}_{ww}^{eq} \tag{13}$$

$$\mathrm{m}_x^{eq} = \mathrm{m}_y^{eq} = \mathrm{m}_z^{eq} = 0 \tag{14}$$

where $\omega_\varepsilon, \omega_{xx}$ and $\omega_{\varepsilon j}$ are the free parameters.

The diagonal collision matrix $\hat{S}$ is:

$$\hat{S} \equiv diag(0, s_1, s_2, 0, s_4, 0, s_4, 0, s_4, s_9, s_{10}, s_9, s_{10}, s_{13}, s_{13}, s_{13}, s_{16}, s_{16}, s_{16}) \tag{15}$$

However, to achieve an optimum stability model Lallemand and Luo[8] obtained the following parameters through linear analysis: $\omega_\varepsilon = 0$, $\omega_{xx} = 0$, $\omega_{\varepsilon j} = -475/63$, $s_1 = 1.19$, $s_2 = s_{10} = 1.4$ $s_4 = 1.2$, $s_{16} = 1.98$ and, the kinematic viscosity ν is given by

$$\nu = \frac{1}{3}\left(\frac{1}{s_9} - \frac{1}{2}\right) = \frac{1}{3}\left(\frac{1}{s_{13}} - \frac{1}{2}\right) \tag{16}$$

MRT models can be reduced to a SRT model by setting all the relaxation parameters to a single relaxation time.

C. LES Form of the Lattice Boltzmann Equation

In LES of turbulent flows, the large scale effects are directly computed, whereas small scale behaviors are represented by subgrid models. The most common approach for modeling subgrid behavior is due to Smagorinsky,[10] which uses an eddy viscosity to represent the small scale energy damping. This model is easy to implement in LBE simulations. The LES-LBE with SRT using the Smagorinsky sub-grid model has been successfully applied to simulate the vortex dynamics in synthetic and free jets, by Menon and Soo.[5] However, this algebraic model has limitations, which can be overcome by the use of the K-eqn. subgrid model. The idea behind the K-eqn. model is to solve for the transport equation of subgrid scale kinetic energy, k^{sgs}, which releases the equilibrium between production and dissipation of kinetic energy needed for the Smagorinsky model.

For the simulations of high Reynolds flows, the LES version of the LBE model is studied. A spatial filter is used to reduce the high wave number components of the particle distribution and separates the resolved scale parts from the unresolved scales. The "filtered" form of the MRT-LBE equation is given by d'Humieres et al.[11]

$$|\overline{f}_\alpha(x_i + e_\alpha \delta t, t + \delta t)\rangle - |\overline{f_\alpha}(x_i, t)\rangle = \quad - M^{-1}\widehat{\overline{S}}[|m(x_i,t)\rangle - |m^{eq}(x_i,t)\rangle], \qquad \alpha = 0, 1, ...18 \tag{17}$$

Here, the distribution function $\overline{f}_\alpha$ represents the filtered particle distribution. The effect of the small scale behavior is modeled through an effective collision term:

$$\nu + \nu_\tau = \frac{1}{3}\left(\frac{1}{s_9} - \frac{1}{2}\right) = \frac{1}{3}\left(\frac{1}{s_{13}} - \frac{1}{2}\right) \tag{18}$$

where ν_τ represents the dissipation effects of the unresolved scales. In this study, this term has been modeled by two sub-grid models, dynamic eddy viscosity model and the dynamic one-equation model for subgrid scale kinetic energy.

1. *Smagorinsky Model*

The simplest model used to close equations for the filtered velocity is the one proposed by Smagorinsky, where the eddy viscosity is given by

$$\nu_\tau = C_s \overline{\triangle^2} \mid S \mid \tag{19}$$

Here C_s is the Smagorinsky constant, which can be determined dynamically, as discussed in the Local Dynamic Model section. $\overline{\triangle}$ is the length scale proportional to the local lattice volume, and $|S| = 2(\overline{S_{ij}}\,\overline{S_{ij}})^{1/2}$ is the large scale strain rate tensor. $\overline{S_{ij}} = \frac{1}{2}(\frac{\partial \overline{u_i}}{\partial x_j} + \frac{\partial \overline{u_j}}{\partial x_i})$ and $\overline{u_i}$ is the large scale velocity.

2. *K-eqn Model*

The transport equation of subgrid kinetic energy $k^{sgs} = 1/2\,(\overline{u_i u_i} - \overline{u_i}\,\overline{u_i})$ is given in the following form

$$\frac{\partial k^{sgs}}{\partial t} + \overline{u_i}\frac{\partial k^{sgs}}{\partial x_i} = -\tau_{ij}^{sgs}\frac{\partial \overline{u_i}}{\partial x_j} - C_\epsilon \frac{(k^{sgs})^{3/2}}{\overline{\triangle}} + \frac{\partial}{\partial x_i}\left(\frac{\nu_\tau}{\sigma_k}\frac{\partial k^{sgs}}{\partial x_i}\right) \tag{20}$$

where τ_{ij}^{sgs} is the modeled subgrid stress tensor,

$$\tau_{ij}^{sgs} = -2\nu_\tau \overline{S_{ij}} + \frac{2}{3}k^{sgs}\delta_{ij} \tag{21}$$

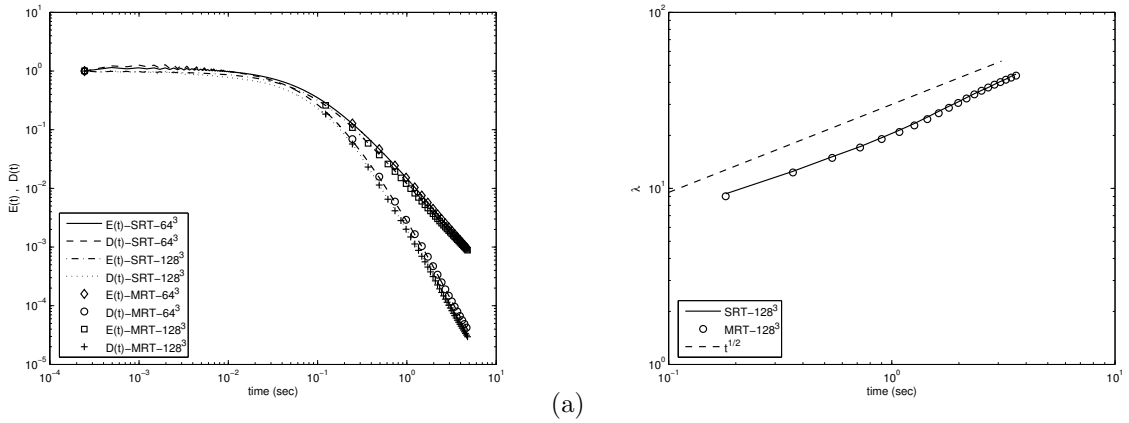

(a) (b)

Figure 2. (a) Time evolution of the normalized kinetic energy and normalized dissipation. (b) Time evolution of the Taylor length scale.

Here ν_τ is the eddy viscosity which is modeled as,

$$\nu_\tau = C_\nu \overline{\triangle} \sqrt{k^{sgs}} \tag{22}$$

where C_ν and C_ϵ are modeled constants, which can also be determined by local dynamic model, ν is the molecular viscosity, and ν_τ is the eddy viscosity at the grid filter level.

In the transport equation of kinetic energy, given in Eqn. (20), the right hand side of equation represents production, dissipation and diffusion of subgrid kinetic energy, respectively. In the flux term σ_k represents the "turbulent Prandtl number" for kinetic energy, which is set to unity at present.

D. Local Dynamic Model

Localized dynamic model is implemented to determine C_s (for the Smagorinsky's model), C_ν, and C_ε model coefficients. The details of this approach are given by Kim et.al. [12,13] The localized dynamic model (LDM) is formulated based on the assumption of the scale similarity in the inertial subrange .[13] The relation for C_ν, as well as C_s, is given as:

$$C_\nu = \frac{\mathrm{L}'_{ij} M_{ij}}{2 M_{ij} M_{ij}} \tag{23}$$

where $L'_{ij} = L_{ij} - \frac{2}{3}\widehat{\overline{\rho}} k^{test} \delta_{ij}$ and $M_{ij} = -\widehat{\overline{\rho}} \sqrt{k^{test}} \widehat{\triangle} (\langle \overline{S_{ij}} \rangle - \frac{1}{3} \langle \overline{S_{kk}} \rangle \delta_{ij})$. Here, $\langle\rangle$ indicates test filtering, $L_{ij} = \widehat{\overline{\rho}} (\langle \overline{u_i u_j} \rangle - \langle \overline{u_i} \rangle \langle \overline{u_j} \rangle)$ is the Leonard stress tensor and $k^{test} = \frac{1}{2} \langle \overline{u_k u_k} \rangle - \langle \overline{u_k} \rangle \langle \overline{u_k} \rangle) = \frac{1}{2} L_{kk} / \widehat{\overline{\rho}}$ is the resolved kinetic energy at the test-filter level. Also, C_ϵ can be obtained from:

$$C_\epsilon = \frac{\widehat{\Delta}(\nu + \nu_\tau)}{(k^{test})^{3/2}} [\langle \overline{T_{ij}} \frac{\partial \overline{u_j}}{\partial x_i} \rangle - \widehat{\overline{T_{ij}}} \frac{\widehat{\partial \overline{u_j}}}{\partial x_i}] \tag{24}$$

The tensor $\overline{T_{ij}}$ is defined as $[\frac{\partial \overline{u_i}}{\partial x_j} + \frac{\partial \overline{u_j}}{\partial x_i} - \frac{2}{3} (\frac{\partial \overline{u_k}}{\partial x_k}) \delta_{ij}]$ and $\widehat{\overline{T_{ij}}}$ indicates the tensor at the test-filter level.

III. Simulation Results

A. LBE-DNS of Decaying Isotropic Turbulence

In order to analyze the ability of the LBE to simulate turbulence, the energy spectrum and the decay characteristics of the energy and the dissipation are studied. Decaying homogeneous isotropic turbulence is simulated using LBE-DNS for both SRT and MRT methods. The resolutions of 64^3 and 128^3 are used with initial Taylor's scale Reynolds number, $Re_\lambda \approx 18$ and 30, respectively. Figure 2 (a) shows the evolution of

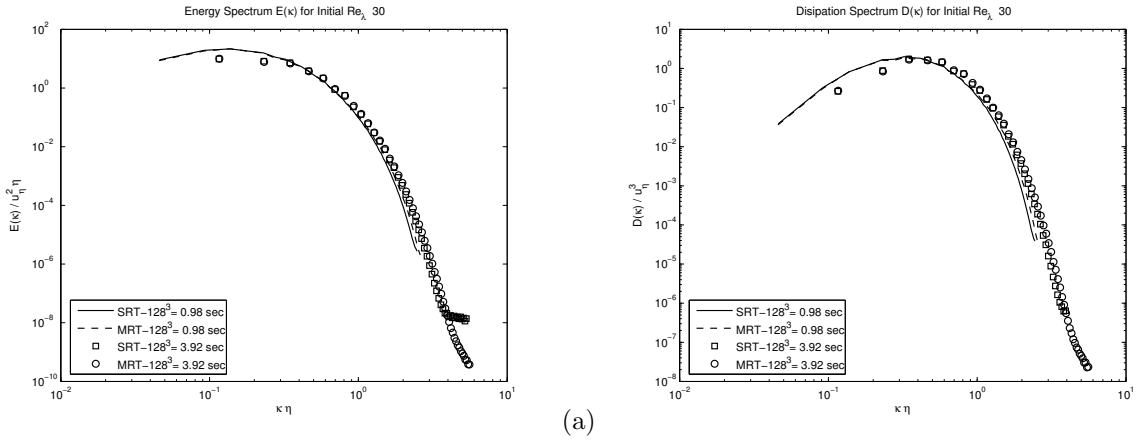

(a) (b)

Figure 3. SRT and MRT-DNS results for decaying isotropic turbulence: (a) Normalized energy spectrum vs. normalized wavenumber, at $t = 0.98sec$ and $t = 3.92sec$. (b) Normalized dissipation spectrum vs. normalized wavenumber at two instants in the decay.

the normalized kinetic energy and the normalized dissipation with respect to time. For decaying turbulence, the kinetic energy and the dissipation are expected to decay as

$$k \propto k_0(t - t_0)^{-n} \tag{25}$$

$$\tag{26}$$

$$\epsilon \propto \epsilon_0(t - t_0)^{-n-1}. \tag{27}$$

The kinetic energy and the dissipation evolution for SRT and MRT are almost identical for both resolutions and initial Reynolds numbers. The kinetic energy and dissipation have decay exponents n close to -1.7 and -2.7, respectively. While it is known that the decay exponents depend on whether the decay is at its beginning or ending period, the decay exponents obtained fall well within the range of classical results,[14,15] Furthermore, for decaying isotropic turbulence, the Taylor scale, λ, should grow with time as $t^{1/2}$. The behavior of λ with time for SRT and MRT is almost identical, and follows closely a 1/2 exponential growth, as shown in Figure 2 (b). Also, from Kolmogorov's first hypothesis, it is known that energy and dissipation spectrum should collapse at high wavenumbers, referred to as universality, for high Reynolds number flows when normalized by the smallest scales of the flow, Kolmogorov's length scales, η, and velocity, u_η. Figure 3 (a) and (b), show the energy and dissipation spectrums, respectively, normalized by Kolmogorov's scales at two different times in the decay. The energy and dissipation spectrums collapse at the high wavenumbers, satisfying Kolmogorov's universality, for both methods SRT and MRT. Also, Figure 3 (a) and (b), show little difference between the MRT and SRT methods.

B. Forced Homogeneous Isotropic Turbulence

Stationary homogeneous isotropic turbulence is simulated using a 64^3 resolution, for MRT and SRT methods, and $Re_\lambda \approx 18$ and 27, respectively. The forcing procedure follows the technique developed by Eswaran and Pope.[16] The statistical moments of the velocity gradient have well-established behavior for stationary isotropic turbulence. Of special interest, are the 3^{rd} and 4^{th} statistical moments, referred to as the skewness and flatness, respectively. The normalized skewness and flatness are

$$S = -\frac{\left\langle \left(\frac{\partial \overline{u}}{\partial x}\right)^3 \right\rangle}{\left\langle \left(\frac{\partial \overline{u}}{\partial x}\right)^2 \right\rangle^{3/2}} \tag{28}$$

$$F = \frac{\left\langle \left(\frac{\partial \overline{u}}{\partial x}\right)^4 \right\rangle}{\left\langle \left(\frac{\partial \overline{u}}{\partial x}\right)^2 \right\rangle^2}. \tag{29}$$

The SRT and MRT methods revealed almost identical mean values for the skewness and flatness factor. The skewness and flatness of the velocity gradient are 0.41 and 3.46, respectively, as shown in Figure 4. These

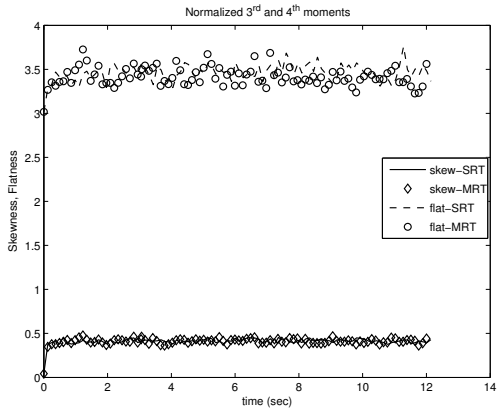

Figure 4. Normalized Skewness and Flatness of the velocity gradient, for forced DNS-MRT and DNS-SRT.

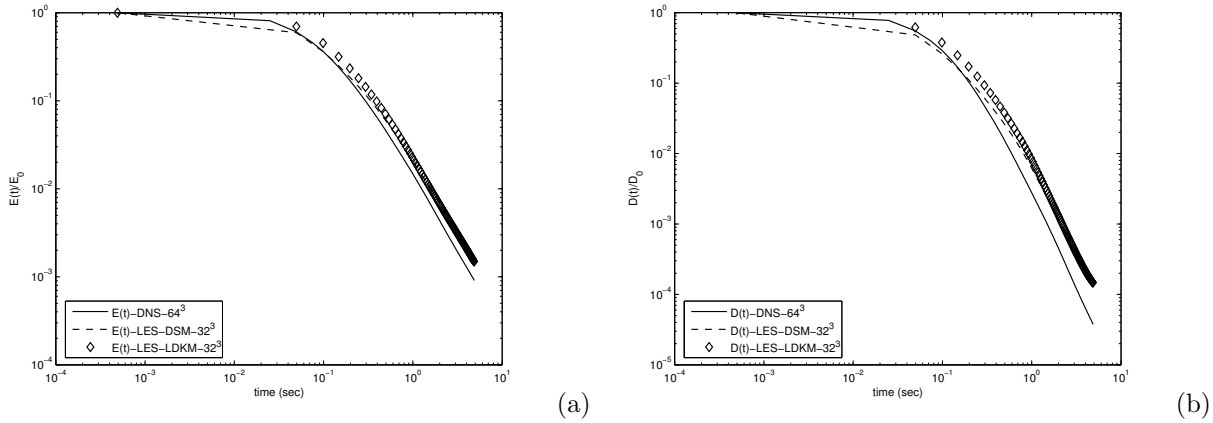

Figure 5. (a) Normalized energy evolution for decaying isotropic turbulence for initial $Re_\lambda \approx 18$. (b) Normalized dissipation evolution for decaying isotropic turbulence for initial $Re_\lambda \approx 18$.

results are in excellent agreement with historical data, see Sreenivasan and Antonia.[17] While for homogeneous isotropic turbulence the SRT and MRT methods seem to reproduce the same physical behavior, there are clear differences and limitations between the two methods, which are discussed further by d'Humieres et al.,[11] and Lallemand and Luo.[8] Furthermore, Krafczyk and Tolke,[18] showed that LES- MRT has better stability and accuracy characteristics than SRT. Therefore, for all the LES studies presented below, the MRT method is used.

C. LBE-LES of Decaying Isotropic Turbulence

Large eddy simulations are performed using dynamic Smagorinsky model (DSM) and localized dynamic K-eqn. model(LDKM). The results of MRT-LBE-LES for decaying isotropic turbulence are presented for a 32^3 grid resolution and an initial $Re_\lambda \approx 18$. The initial velocity field for the LES is obtained from the DNS data. Figures 5 (a) and (b) show, respectively, the time evolution of the normalized kinetic energy and dissipation. The dynamic Smagorinsky model underpredicts the energy and dissipation of the DNS in the initial portion of the decay. Also, at the beginning of the decay, the LES-DSM has a lower energy and dissipation decay rate than the DNS. On the other hand, the LDKM shows the same initial energy and dissipation level as the DNS, but both, energy and dissipation start to decay at a later time than the DNS. However, the LDKM shows a similar decay rate as the DNS for both energy and dissipation at all times.

The energy and dissipation spectrum of the LES and DNS are compared in Figures 6 (a) and (b). At

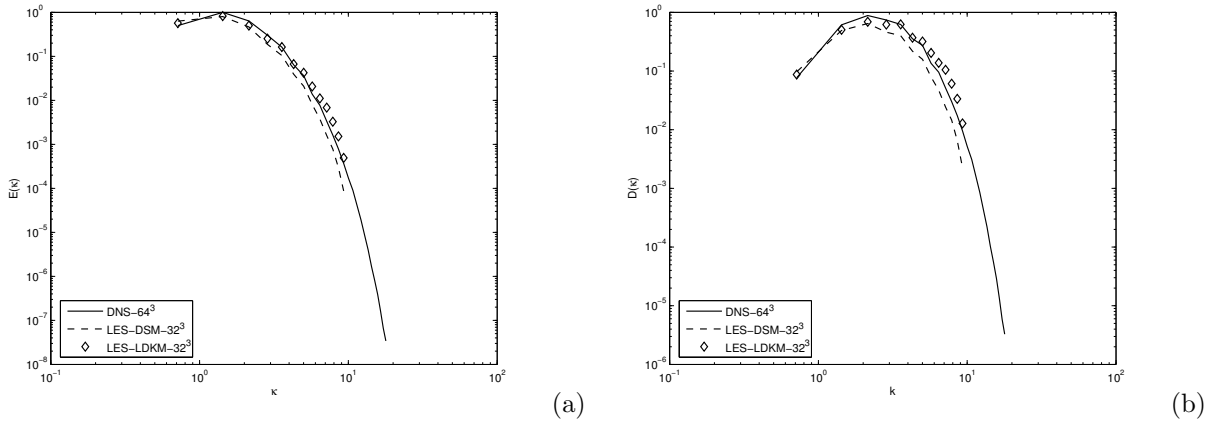

Figure 6. (a) Energy spectrum, as a function of wavenumber κ at $t = 0.98sec$. (b) Dissipation spectrum, as a function of wavenumber κ at $t = 0.98sec$.

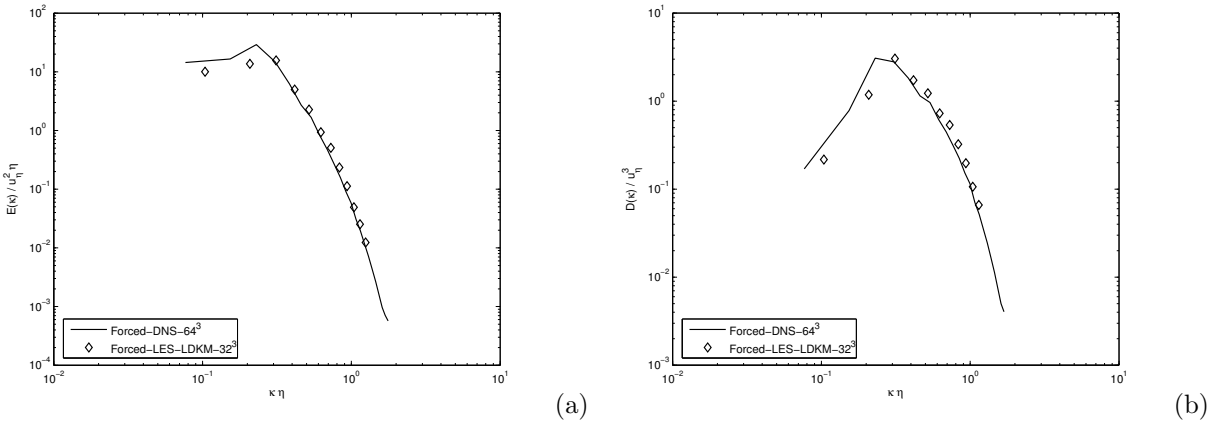

Figure 7. (a) Energy spectrum, nomalized by u_η, as a function of wavenumber, normalized by η. (b) Dissipation spectrum, normalized by u_η, as a function of wavenumber, normalized by η.

higher wavenumbers, representing the small scales, the LDKM has more energy than the DNS. On the other hand, the Dynamic Smagorinsky underpredicts the DNS spectrum for a wide range of wavenumbers. Similarly, for the dissipation spectrum, at the small scales, the LDKM shows a higher dissipation than the DNS, while the DSM shows a lower dissipation than DNS. Despite those differences, both models provide a good approximation to the DNS spectrums.

D. LBE-LES of Forced Isotropic Turbulence

Forced MRT-LES with K-eqn. model is performed and results are compared with those of forced DNS, for $Re_\lambda \approx 18$. The normalized energy and dissipation spectrum are shown in Figures 6 (a), and (b), respectively. Since the initial velocity field for the LES was obtained from the DNS data, without truncating the high wavenumbers form the energy spectrum, there is a slight desagreement beteween the LDKM and DNS at low wavenumbers, corresponding to the large scales. However, the LDKM shows an excellent agreement with the DNS for the energy and dissipation spectrums at the high wavenumbers.

Also, it is of interest to compare the skewness and flatness of the velocity gradients of the LES and DNS. Figure 8 shows the normalized skewness and flatness factor of the velocity gradient for the DNS, and LDKM. The LDKM has a mean skewness and flatness of 0.29 and 3.1, respectively, which represent a 30 and 10 percent difference, respectively, as compared with the DNS mean values.

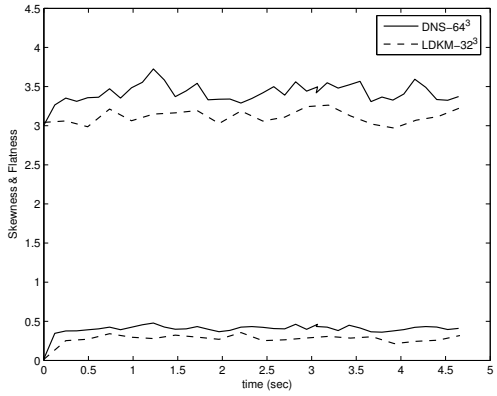

Figure 8. Skewness and flatness of the velocity gradient for forced LES and DNS.

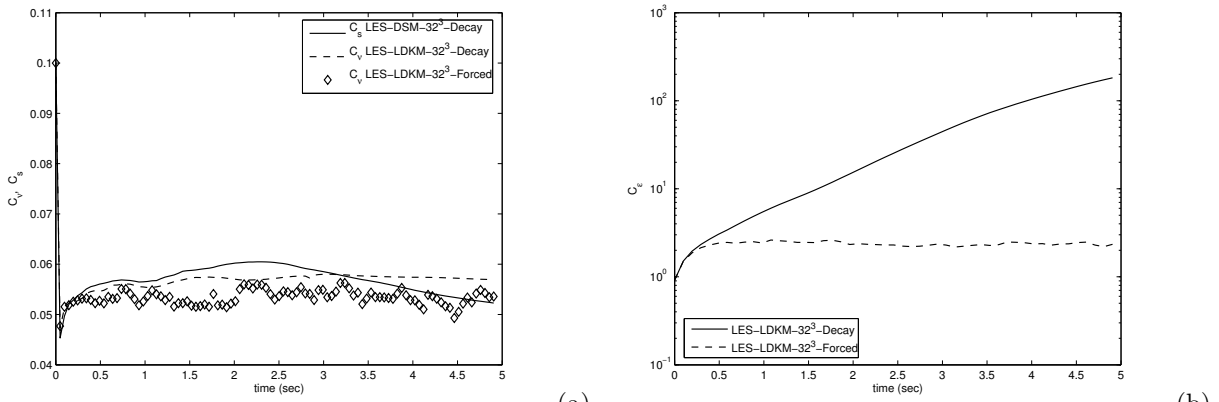

(a) (b)

Figure 9. (a) Time evolution of C_ν and C_s for forced LES and decay LES. (b) Time evolution of C_ϵ for forced and decay LES-LDKM.

Using the the local dynamic model, the appropriate value of C_ν, C_s, and C_ϵ are calculated according to equation (23). Figure 9 (a) shows the variation of C_ν and C_s with time. After an unphysical, transient initial period, C_ν and C_s stabilize close to 0.005. For decaying LES-DSM the value of C_s is fairly constant in time, and then, as expected, it starts to decrease slowly as the turbulence decays. On the other hand, the C_ν, corresponding to LDKM, remains almost constant. Also, for forced LES-LDKM the value of C_ν remains statistically steady with time. Another coefficient that is dynamically calculated is C_ϵ in the LDKM method. For decaying turbulence, C_ϵ increases rapidly, to ensure that any subgrid kinetic energy is produced dissipates at a faster rate, see Figure 9 (b). On the other hand, C_ϵ reaches a statistically steady value for the forced LDKM, as expected. In the LES-LDKM method the subgrid kinetic energy k^{sgs} is calculated by solving equation (20). For the decaying turbulence, the small scales start to grow as the energy from the small scales, k^{sgs}, is dissipated rapidly, causing the subgrid kinetic energy to drop, as shown in Figure 10 (a) However, for forced LDKM, the k^{sgs} decreases until the small scales reach a steady kinetic energy level through the cascade process, evidenced by a constant k^{sgs} value at later times. Also, for the forced K-eqn. model the production and dissipation terms reach a steady state, while for decaying LDKM the production and dissipation decrease monotonically with time, as shown in Figure 10 (b). Finally, Figure 11 shows the typical vortical structures in the flow, revealed by the contours of the vorticity magnitude ($|w| = 0.0055$), and contour levels of C_ν for forced LDKM.

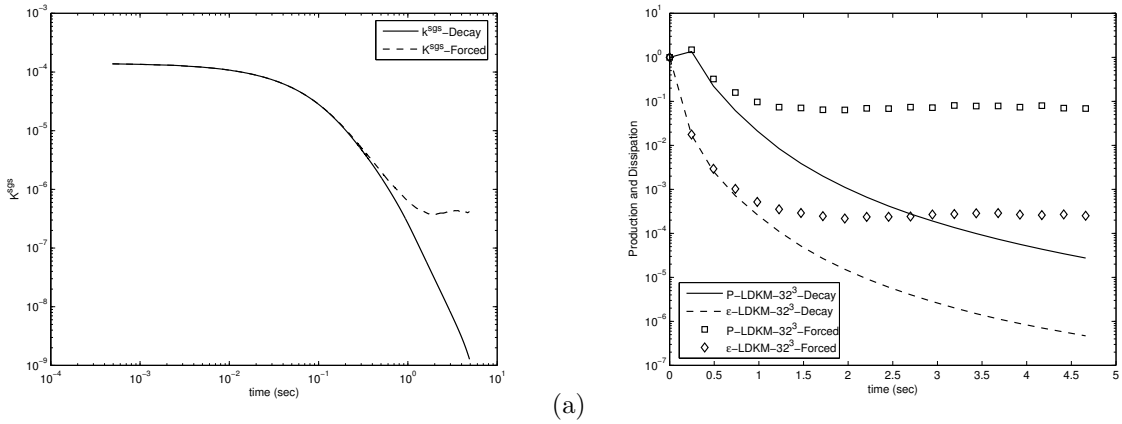

(a) (b)

Figure 10. (a) Time evolution of K^{sgs} for forced and decay LES-LDKM. (b) Normalized production and negative of the dissipation for forced LES-LDKM.

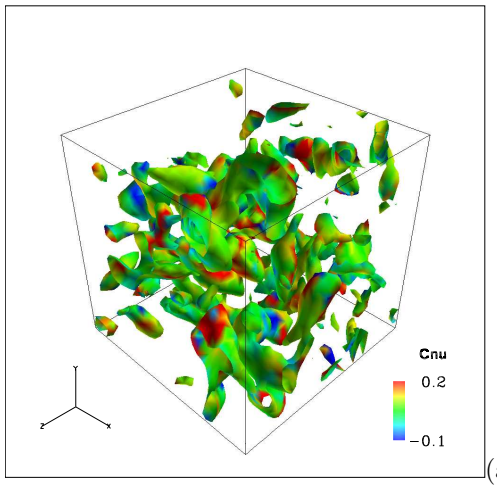

(a)

Figure 11. (b) Vorticity magnitude contours ($|w| = 0.0055$), with C_ν contour levels for forced LDKM.

IV. Conclusion

The lattice Boltzmann method is used to perform DNS and LES for decaying and forced of homogeneous isotropic turbulence. First, LBE-DNS is performed for two cases with resolutions, 64^3 and 128^3 , and with $Re_\lambda \approx 18$ and 30, respectively. The LBE-DNS results are presented for both SRT and MRT, which resulted in almost identical behavior. Also, the LBE-DNS of decaying homogeneous isotropic turbulence is able to reproduce the well known power law decay rates for the energy and dissipation. Moreover, the energy and dissipation spectrums for decaying turbulence collapse well when normalized by Kolmogorov's scales, considering the low Reynolds numbers analyzed. Second, forced LBE-DNS is performed. The 3^{rd} and 4^{th} statistical moments of the velocity gradient are in excellent agreement with many previous studies.[17] Third, lattice Boltzmann method is used to perform LES with a 32^3 resolution for an $Re_\lambda \approx 18$ using dynamic Smagorinsky and the dynamic K-eqn. model. For decaying homogeneous isotropic turbulence, both methods provide very good agreement with the spectral characteristics of the energy and the dissipation as compared with DNS. Finally, forced LES is performed using the K-eqn. model for a 32^3 resolution and $Re_\lambda \approx 18$, and compared with forced LBE-DNS with a 64^3 resolution and the same Reynolds number. The energy and dissipation spectrums of the forced LES are shown to reproduce well the DNS spectrums. Despite the poor resolution of the LES, it is able to capture some of the characteristics of the 3^{rd} and 4^{th} statistical moments

of the velocity gradient. While the agreement is not perfect, the magnitude of the skewness and flatness are approximated. However, as a property of filtered fields in general, the skewness and flatness are closer to the Gaussian values of 0 and 3, respectively. The LBE has proven to reproduce the important features of turbulence, and has been successfully adapted for forced LES using the K-eqn. model. The promising results obtained here, will allow the LBE-LES with K-eqn. model to be used in other applications such as wall bounded flows.

V. Acknowledgements

This work was supported in part by the Office of Naval Research. Computer time was provided by DOD HPC center at NAVO, ERDC and ARL are gratefully acknowledged.

References

[1]He, X. and Luo, L. S., "A priori derivation of the lattice Boltzmann equation," *Physical Review E*, Vol. 55, No. 6, 1997, pp. R6333–R6336.

[2]He, X. and Luo, L. S., "Theory of the lattice Boltzmann method: From the Boltzmann equation to the lattice equation," *Physical Review E*, Vol. 56, No. 6, 1997, pp. 6811–6817.

[3]Takashi, A., "Derivation of the Lattice Boltzmann method by means of the discrete ordinate method for the Boltzmann equation," *Journal of Computational Physics*, Vol. 131, 1997, pp. 241–246.

[4]Yu, D., Mei, R., Luo, L.-S., and Shyy, W., "Viscous flow computations with the method of lattice Boltzmann equation," *Progress in Aerospace Sciences*, Vol. 39, 2003, pp. 329–367.

[5]Menon, S. and Soo, J.-H., "Simulation of vortex dynamics in three-dimensional synthetic and free jets using the large-eddy lattice Boltzmann method," *Journal of Turbulence*, Vol. 5, 2004, pp. 1–26.

[6]Feiz, H. and Menon, S., "LES of multiple jets in crossflow using a coupled lattice Boltzmann-finite volume solver," *AIAA Paper 03–5206*, 2003.

[7]d'Humieres, D., "Generalized lattice Boltzmann equations in: Rarefied Gas Dynamics: Theory and Simulations," *Prog. Astronaut. Aeronaut.*, Vol. 159, 1992, pp. 450–458.

[8]Lallemand, P. and Luo, L. S., "Theory of the lattice Boltzmann method: Dispersion, dissipation, isotropy Galilean invariance, and stability," *Physical Review E*, Vol. 61, 2000, pp. 6546.

[9]Krafczyk, M. and Tolke, J., "Large-eddy simulations with a multiple-relaxation-time LBE model," *International Journal of Modern Physics B*, Vol. 17, 2003, pp. 33–39.

[10]Smagorinsky, J., "General Circulation Experiments with the Primitive Equations," *Monthly Weather Review*, Vol. 91, No. 3, 1993, pp. 99–164.

[11]d'Humieres, D., Ginzburg, I., Krafczyk, M., Lallemand, P., and Luo, L., "Multiple-relaxation-time lattice Boltzmann models in three dimensions," *Phil. Trans. R. Soc. Lond.*, Vol. 360, 2002, pp. 437–451.

[12]Kim, W.-W., Menon, S., and Mongia, H. C., "Large eddy simulations of a gas turbine combustor flow," *Combustion Science and Technology*, Vol. 143, 1999, pp. 25–62.

[13]Kim, W.-W. and Menon, S., "An unsteady incompressible Navier-Stokes solver for Large-Eddy Simulation of turbulent flows," *International Journal of Numerical Fluid Mechanics*, Vol. 31, 1999, pp. 983–1017.

[14]Huang, M.-J. and Leonard, A., "Power-law decay of homogenous turbulence at low Reynolds numbers," *Physics of Fluids*, Vol. 6, No. 11, 1994, pp. 3765–3775.

[15]Skrbek, L. and Stalp, S., "On the Decay of Homogeneous Isotropic Turbulence," *Physics of Fluids*, Vol. 12, No. 8, 2000, pp. 1997–2019.

[16]Eswaran, V. and Pope, S. B., "An examination of forcing in direct numerical simulations of turbulence," *Computers and Fluids*, Vol. 16, 1988, pp. 257–278.

[17]Sreenivasan, K. R. and Antonia, R. A., "The Phenomenology of Small-Scale Turbulence," *Annu. Rev. Fluid Mechanics*, Vol. 29, 1997, pp. 435–472.

[18]Yu, H. and Girimaji, S., "Near-field turbulent simulations of rectangular jets using lattice Boltzmann method," *Physics of Fluids*, Vol. 17, No. 12, 2005, pp. 125106–17.